RESEARCH ARTICLE
doi: 10.2306/scienceasia1513-1874.2022.152

ScienceAsia 49 (2023): **169–176**

Prediction of substrate binding on mobile colistin resistance using *in silico* approach

Chonnikan Hanpaibool[a], **Phornphimon Maitarad**[b], **Thanyada Rungrotmongkol**[a,c,*]

[a] Center of Excellence in Biocatalyst and Sustainable Biotechnology, Department of Biochemistry, Faculty of Science, Chulalongkorn University, Bangkok 10330 Thailand

[b] Research Center of Nano Science and Technology, Department of Chemistry, College of Science, Shanghai University, Shanghai 200444 China

[c] Program in Bioinformatics and Computational Biology, Graduate School, Chulalongkorn University, Bangkok 10330 Thailand

[*]Corresponding author, e-mail: thanyada.r@chula.ac.th

Received 22 May 2022, Accepted 11 Oct 2022
Available online 5 Dec 2022

ABSTRACT: Colistin, an antibiotic, has become a last-resort therapy for serious infections caused by Antimicrobial Resistance (AMR) diseases during the last decade. The positively charged colistin coupled to the negatively charged lipid A can rupture the outer cell membrane of Gram-negative bacteria. However, the presence of a mobile colistin resistance gene (*mcr* gene) in Enterobacteriaceae has resulted in colistin resistance. MCR function transfers phosphoethanolamine (PEA) of phosphatidylethanolamine (PE) to lipid A, neutralizing its negative charge and preventing the binding of positively charged colistin. Currently, *mcr* isoforms varied from *mcr-1* to *mcr-10* have been discovered in environmental and clinical isolates, but only the three-dimensional structures of the catalytic portion of two MCR proteins, MCR-1 and MCR-2, were crystallized. Full-length MCR protein structures may be necessary for understanding MCR function and developing inhibitors; therefore, the structures of MCR-1 to 10 proteins were predicted by novel accurate protein prediction utilizing Deep Learning (RoseTTAFold). Based on multiple-sequence alignment and superposition on all MCR protein structures, there are six conserved residues at the active site, HIS^1, HIS^2, HIS^3, ASP, GLU, and THR. Tunnel analysis was utilized to determine the possible routes for substrate PE entering into MCR proteins. Among the four substrate-binding paths to the MCR active site (tunnels 1–4), PE preferentially binds at the active site via tunnel 1. This discovery not only anticipates PE as a substrate-binding to MCR protein, but it might also be beneficial for guiding MCR inhibitors.

KEYWORDS: colistin, phosphatidylethanolamine, RoseTTAFold, CAVER, antimicrobial resistance

INTRODUCTION

Antimicrobial resistance (AMR) is one of the worldwide public health problems. By 2050, AMR infection could lead to more than 10 million deaths annually (World Health Organization, 2019). Especially, AMR was found to be particularly common in bacteria that can cause infections in humans and animals [1]. However, it takes a decade to produce a new drug to tackle resistant bacterial strains [2]. Over the past decade, colistin has been regarded as one of the few antibiotics to exhibit significant efficacy against Gram-negative bacteria; then, it has become a last-resort treatment for acute AMR infection [3]. Because of its crucial role as the last line of defense in treating diseases caused by resistant pathogenic organisms, the widespread of colistin resistance among bacteria has recently gained extensive attention [4]. Typically, the Gram-negative bacteria's outer cell membrane can be disrupted by the positively charged colistin linked to the negatively charged lipid A [5]. Colistin binds to lipid A of lipopolysaccharides (LPSs) by replacing calcium and magnesium from Gram-negative bacteria's outer cell membrane, causing cell membrane permeability changes and cell content leakage [1]. However, the existence of a mobile colistin resistance gene (*mcr* gene) in Enterobacteriaceae can cause colistin resistance [6]. It has been reported that MCR protein, which was encoded by *mcr* gene, works as a phosphoethanolamine (PEA) transfer reaction to lipid A on the Gram-negative bacterial outer membrane [7], neutralizing the bacterial membrane's negative charge and reducing colistin binding [8]. The presence of modified lipid A reduces colistin affinity, making the antibiotic ineffective and causing bacteria resistance [9].

Up to date, there are ten different versions of the *mcr* gene (*mcr-1* to *mcr-10*) found in bacteria from various sources, including humans, animals, and the environment [10, 11]; however, only the catalytic domains of MCR-1 and MCR-2 have been reported in the PDB databank. The full-length crystal structure of lipid A phosphoethanolamine transferase (EptA), which belongs to the same protein family as MCRs, suggested that the transmembrane domain is also needed for PEA hydrolysis [12]. Herein, we aimed to predict the full-length protein structures of MCR-1 to 10 utilizing RoseTTAFold on the Robetta server, a revolutionary deep learning algorithm technique for getting more accurate structure prediction [13]. All of the ten MCR structures (MCR-1 to 10) were examined,

emphasizing conserved active site residues to identify critical residues for MCR activity. Furthermore, the tunnels through the MCR active site were studied by the geometry-based tunnel prediction program CAVER 3.03, while the binding of substrate phosphatidylethanolamine (PE) was predicted by molecular docking.

MATERIALS AND METHODS

Structure prediction of MCR-1 to 10

MCR protein sequences of MCR-1 (WP 049589868), MCR-2 (WP 065419574), MCR-3 (WP 039026394), MCR-4 (WP 099156046), MCR-5 (WP 053821788), MCR-6 (ASK49942), MCR-7 (WP 104009851), MCR-8 (AVX52225), MCR-9 (WP 001572373), and MCR-10 (WP 023332837) obtained from the National Center for Biotechnology Information (NCBI) were employed for an investigation of their three dimensional (3D) structures. The ClustalW was used to examine the multiple sequence alignment (MSA) of all MCR variants on GenomeNET (https://www.genome.jp), while their identity percentage was calculated by BLASTp [14]. MSA of homologous proteins was displayed by ESPript, a well-known sequence alignment renderer [15]. RoseTTAfold on the Robetta server [13] was used to generate molecular models of the ten MCR proteins. The top five scoring models for each prediction run were generated. The top five scoring models were all similar, the only difference being the low-confidence and likely unfolded portions were found at the proteins' extreme N- and C-termini. Thus, the top-scoring predicted protein structure was then chosen. The ChimeraX tool displayed mapping sequence conservation onto MCR structures [16]. The Zn binding site was predicted using the Metal Ion-Binding site prediction (MIB) (https://bioinfo.cmu.edu.tw/MIB) [17]. Because the Zn ion location was discovered to be in the same place as the MCR-1 crystal structure, the Zn ions were added to all MCR variations by superposition with the MCR-1 catalytic domain (PDB ID: 5LRN) [18].

Computational analysis of MCR tunnels

The tunnels allow tiny molecules, ions, and water solvents to move through a wide range of proteins. Using the geometry-based tunnel prediction program CAVER 3.03 [19], the tunnels have been postulated as paths for substrate migration and putative inhibitor pathways in MCR. The radius of the CAVER settings was set to their default values, and the binding site was chosen as the beginning point. For all identified tunnels heading to the active site, the bottleneck radius referring to the maximal probe size of the narrowest part of the tunnel [20] was analyzed and compared. Note that the transport of small molecules to the binding pocket cannot be taken place through the tunnel with a relatively narrow bottleneck radius. Additionally, ChimeraX [16] were used to create the visualization of their tunnel.

Molecular docking of PE substrate

The 3D structure MCR substrate, phosphatidylethanolamine (PE), retrieved from the ZINC database [21] (ZINC32837869) [22], was randomly docked into the prepared MCRs using the SwissDock server [23]. The missing hydrogen atoms of protein and ligand were added by the Chimera 1.16 program [24]. The blind docking simulation was used to determine all possible PE binding on MCR protein. The intermolecular interaction of the docked PE-MCR complex with the lowest binding free energy was characterized using the LigPlot^{+} v.2.2.5 program [25]. In addition, ChimeraX was utilized to construct all 3D structures of MCRs with and without PE bound.

RESULTS AND DISCUSSION

Modeled structures of MCRs

Since the report of *mcr-1* discovery in November 2015 [26], multiple variations of the gene have been identified, including *mcr-1*, *mcr-2*, *mcr-3*, *mcr-4*, *mcr-5*, *mcr-6*, *mcr-7*, *mcr-8*, *mcr-9*, and *mcr-10*. The most recently identified *mcr* gene, the *mcr-10*, was discovered in 2020 [27]. Multiple sequence alignment (MSA) were used to examine their relationships. The supplemental Fig. S1 shows the percentage of identity when comparing all ten MCR protein sequences in a range of 33.0–87.9. MCR-2 and MCR-6 have the highest percent identity in protein sequence (87.9%), whereas MCR-1 and MCR-2 have an 81.3% identical relationship. Apart from MCR-1 and MCR-6, which have 82.8% identity, MCR-1, MCR-2, and MCR-6 have the highest protein sequence similarity; and MCR-9 and MCR-10 matched 82.9% of identity. The relationships of MCR-3 with MCR-7, MCR-9, and MCR-10 are 71.6, 64.7, and 62.1%, respectively. While MCR-4, MCR-5, and MCR-8 have less than 50% identification with the other MCR types.

From the MSA results for transmembrane and periplasmic domains of the ten studied MCRs (Fig. S2 and Fig. S3), the conserved consensus residue was more concentrated in the periplasmic domain (see also the superimposed MCR structures in Fig. 1A). The 3D structures of all obtained models were well aligned with the full-length X-ray structure of EptA with substantially conserved PH2 and PH2' as a periplasmic-facing domain which played an important role in substrate binding (Fig. S4A) [12]. In particular, the active site residues were located in the same place and were preserved entirely in all MCRs and EptA, as shown in Fig. 1B and Fig. S4A. There are six conserved residues: HIS^{1}, HIS^{2}, HIS^{3}, ASP, GLU, and THR. By using the Metal Ion-Binding site prediction (MIB) [17], the Zn ions were predicted to be coordinated with these conserved residues (Fig. 2A) in good agreement

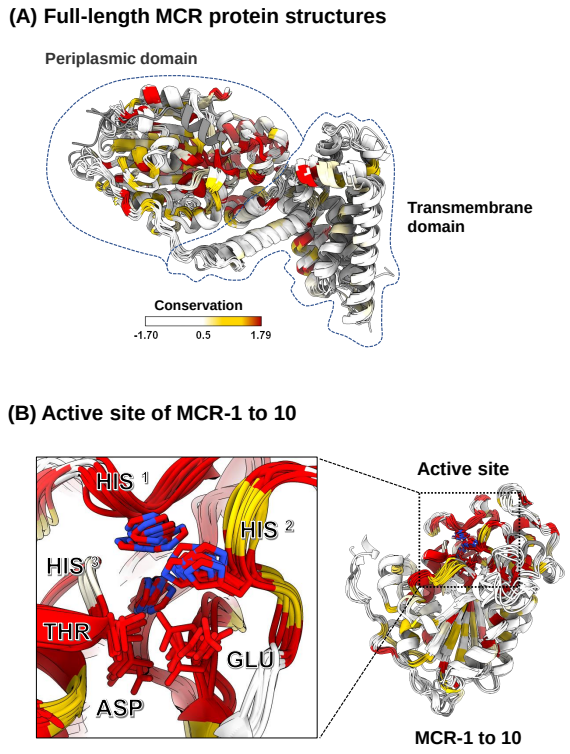

	HIS[1]	HIS[2]	HIS[3]	ASP	GLU	THR
MCR-1	478	395	466	465	246	285
MCR-2	476	393	464	463	244	283
MCR-3	463	380	451	450	238	277
MCR-4	465	382	453	452	240	278
MCR-5	471	389	459	458	248	286
MCR-6	476	393	464	463	244	283
MCR-7	461	378	449	448	236	275
MCR-8	471	388	459	458	243	282
MCR-9	463	380	451	450	238	277
MCR-10	463	380	451	450	238	277

Fig. 1 (A) Superimposition of MCR protein structures modelled by RoseTTAfold [13], while their consensus conserved residues among the ten MCRs (MCR-1 to 10) with 100% and 70% identity are shaded by red and yellow, respectively. (B) The six conserved residues located in the MCR active site are listed below.

Fig. 2 (A) Zn-ion binding at the active site of modelled MCRs resulted from the MIB server [17]. (B) The Zn^{2+} ions bound to the active site of MCR-1 and MCR2 crystal structures where the score for metal-binding position is shown in the green box [18, 28]

with the crystallographic structures of the MCR-1 and MCR-2 periplasmic domain [18, 28] (Fig. 2B). The site-directed mutagenesis-based assay on these six residues critical for the activity of MCR-1 (E246, T285, H395, D465, H466, and H478) and MCR-2 (E244, T283, H393, D463, H464, and H476) suggested essential functions in the maintenance of MCR-1 and MCR-2's biochemical mechanism and colistin-resistant phenotype [8, 29–31]. Furthermore, these residues were in a putative zinc-binding/catalytic motif on MCR-1 and MCR-2 [18, 28]. Consistent with our findings, the six conserved residues may play an essential role in the MCR family's activity. Notably, the well-aligned 3D structures of the periplasmic domain between our predicted models and the crystal structures of MCR-1 and MCR-2 with RMSD of 0.933 Å and 0.936 Å, respectively, were depicted in Fig. S5.

Protein tunnels

Tunnel analysis was utilized to determine the possible routes for ligand entry into MCR proteins. To quantify the tunnel, the radius of the tunnel leading to the binding pocket in the MCR structures was calculated using the Caver 3.0 software, which is widely used for the identification and characterization of transport pathways in macromolecular structures [19]. All possi-

(A) Possible tunnels

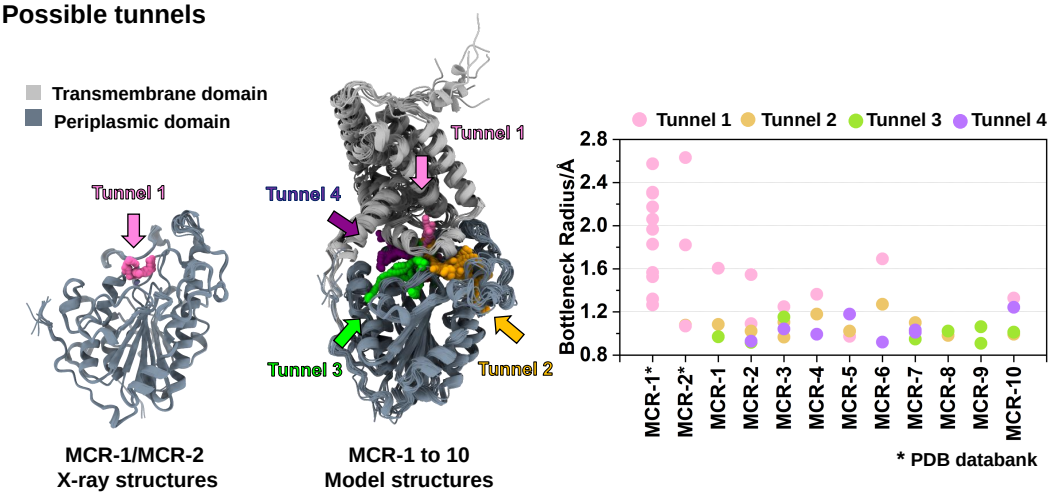

(B) Tunnel 1-lining residues

MCR-1	MCR-2	MCR-3	MCR-4	MCR-5	MCR-6	MCR-7	MCR-8	MCR-9	MCR-10
	V87				V87				V84
	T88								
F93	F91			F 97	F91	A86	F92	S88	A88
Y97	Y95			Y 101		Y90		Y92	
T99	T97		V95	V 103	T97	V92		V94	V94
Y101	Y99		F97		Y99	F94		F96	F96
T104	T102		G100	A 108		S97			S99
M105	M103	M100	M101	M 109	M103	M98	M104	M100	M100
L106	L104			L110	L104				I101
Q107	Q105				Q105		Q106		E102
N108	N106	N103	N104	N 112	N106	N101	N107	N103	N103
A109	A107	I104	T105	L 113	A107	I102	F108	I104	I104
L110	M108		F106	M 114	L108				L105
	Q109				Q109		E110	E106	
T112	T110	T107	T108	T116	T110	T105	T111	T107	T107
	D111			D 117	D111				
E116	E114	E111	112 GLU	E 120	E114		E115	E111	E111
T117	S115	A112	A113	A 121	S115	A110	L116	A112	A112
		L113		S 122					
L120	L118	Y115	Y116	L124	L118	Y113	Y119	Y115	Y115
	M119			L 125	M119		L120		
	F123								L120
									Y194
	E244				E244		E243	E238	
								T239	
		T275	T276	T 284		T273	T280	T275	T275
S284	S282	A276	A277	D 285	S282	A274	A281	A276	A276
	T283	T277	T278	T 286	T283	T275	T282	T277	T277
	A284	A278	A279	A 287	A284	A276	A283	A278	A278
					Y285				
	N327				N327		N326	D321	
	S328				S328				
	K331				K331		K331	K325	
H395	H393	H380	H382	H 389	H393	H378	H388	H380	H380
G396	G394	G381	G383	G 390	G394	R379			G381
P397	P395			P 391	P395	P380			P382
		D450						D450	
	H464	H451			H464		H459	H451	
L477	L475		L464	L 470	L475	L460	L470	L462	L462
H478	H476	H463	H465	H471	H476	H461	H471	H463	H463
G479		G464	G466	G 472	G477	G462	G472	G464	G464
			A467	I 473		T463			T465
									A278
									G381

Fig. 3 (A) Possible tunnels of MCR-1/MCR-2's X-ray structures and the full-length MCRs calculated by CAVER 3.0 where their bottleneck radii are given in the scatter plot compared to those of the crystal structures of the MCR-1 (PDB id: 5LRN [32], 5LRM [32], 5GRR [33], 5K4P [34], 5YLC [35], 5YLE [35], 5YLF [35], 5ZJV [39], 6LI4 [36] and 6LI5 [36]) and MCR-2 (PDB id: 5MX9 [28], 6A7W [37] and 6SUT [38] periplasmic domain. (B) Comparison of tunnel-lining residues on tunnel 1 among the ten MCR variants (residues within the 3.0 Å distance from the tunnel). The tunnel 1-lining residues found in the MCR-1 and MCR-2 crystal structures [28, 32, 37, 38] are underlined.

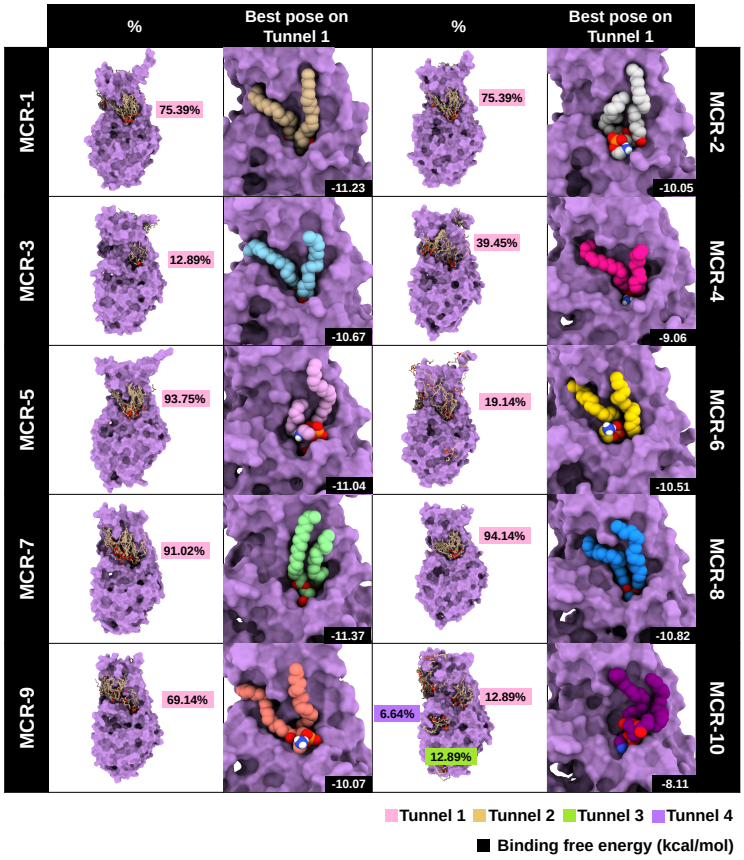

Fig. 4 The percentage of PE substrate binding to the tunnels 1 to 4 with the best docked pose on the tunnel 1 retrieved by blind docking simulation on the ten MCR models using the SwissDock server [23], where the substrate-protein interactions are depicted in Fig. 5.

ble routes for ligand access to the binding site of the ten MCR proteins were illustrated in Fig. 3A. Four different routes were predicted for ligand access to the MCR protein (tunnels 1 to 4), each of which clearly showed a separate track heading to the active site. Each tunnel has an independent bottleneck radius providing the tunnel's narrowest point. The ligand access from a bulk solution to the protein's active site is more favorable in the tunnel with a large bottleneck radius. On the other hand, the relatively small radius could prevent the ligand access to the binding pocket. The scatter plot of bottleneck radii of tunnels revealed that tunnel 1 had the most extensive bottleneck radius in all MCRs except for MCR-5. The bottleneck radius in tunnel 1 was 1.60, 1.55, 1.25, 1.36, 0.97, 1.69, 1.10, 1.02, 1.06, and 1.33 Å for MCR-1 to 10, respectively, which can be enlarged to 2.57 and 2.63 Å in the crystal structures of MCR-1 and MCR-2 without transmembrane domain [28, 32–39]. In addition, only tunnel 1 was found in the X-ray structures of MCR-1, MCR-2 and EptA periplasmic domains, while six tunnels were detected in the full-length EptA structure (Fig. 3A and Fig. S4B). Among them, the tunnel 1 with the largest tunnel radii and shortest length could serve as the most probable substrate binding pathway.

The tunnel-lining residues on tunnel 1 for the ligand-binding route traveled through the crucial His^1/His^2 active site residues shared several conserved residues in all MCR types as follows: M105, N109, T112, H395 (His^1), and H478 (His^2) with residue number according to MCR-1 in Fig. 3B. Some tunnel 1-lining residues were also found in the crystal structures of MCR-1 (S284, H395, G396, H478, and G479) and MCR-2 (E244, S282, T283, N327, S328, K331, H393, G394, P395, H464, L475, and H476) [28, 37, 38].

PE substrate binding to MCRs

The PE substrate binding to MCRs was studied by blind docking simulation using the SwissDock server [23]. The percentage of PE substrate binding to the four tunnels and the PE conformation with the highest binding affinity at tunnel 1 were shown in Fig. 4. It can be seen that the majority of PE were situated on the tunnel 1 close to the active site of MCR-1 (75.39%), MCR-2 (75.39%), MCR-5 (93.75%), MCR-7 (91.02%), MCR-8 (94.14%), and MCR-9 (69.14%). Although

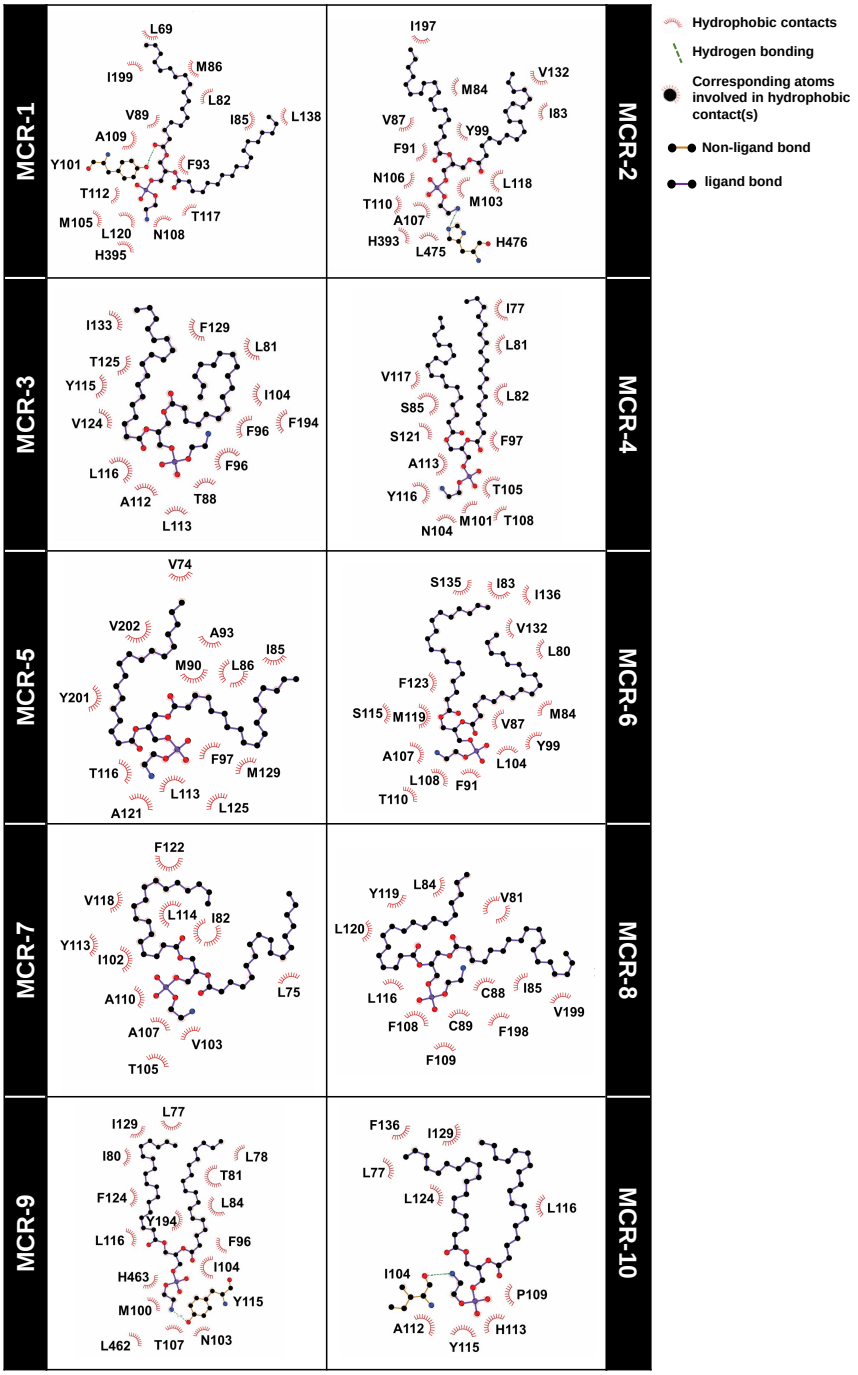

Fig. 5 2D diagram of substrate-protein interactions in the PE-MCRs complexes computed by LigPlot^{+} 2.2.5.

the possibility of PE binding to this tunnel of MCR-3, MCR-4, and MCR-6 was less than 40%, no poses were identified on any other tunnel. For MCR-10, PE was found at the tunnels 1 (12.89%), 3 (12.89%) and 4 (6.64%).

The binding free energy of the best PE docked pose in tunnel 1 ranged from −8.11 to −11.37 kcal/mol for all studied MCRs (Fig. 4). In tunnel 1, the PEA group of PE was likely accommodated in almost the same pocket close to the active site in the periplasmic domain, while the long-chain fatty acid laid on the transmembrane domain. As expected, PE could bind with MCRs mainly

through hydrophobic contacts, while a hydrogen bond stabilized the hydrophilic group in MCR-1, MCR-2, MCR-9, and MCR-10 (Fig. 5). The PE headgroup was bound to PH2/PH2' helices (residues 100–112) consistent with the previous molecular dynamics study on EptA [12]. Interestingly, the PEA group of PE showed interactions with the critical residues H395 in MCR-1, H393/H476 in MCR-2, and H463 in MCR-9. The alanine scanning site-direct mutagenesis of MCR-1 and MCR-2 on the active site residues using colistin susceptibility assays revealed that replacing the conserved H395/H393 and His478/H476 might lower colistin MIC to basal values [31, 40, 41]. These two MCRs have specified the genetic necessity for a substrate-binding/catalytic domain. Our findings might reflect that His^1 and His^2 were vital residues for PE binding in MCRs. The obtained results well agreed with the docked PE/EptA structure (Fig. S7), in which the majority and the best pose of PE binding were situated on tunnel 1 with a similar orientation and binding affinity (−10.16 kcal/mol). Hydrophobic contacts and hydrogen bond interactions could support the PE binding, especially with the crucial residues H465 and H383. However, the structural dynamics are generally required for ligand access to the binding pocket [42–44], i.e., the substrate could bind deeper and interact better into the active site.

CONCLUSION

After discovering ten *mcr* genes (*mcr-1* to *10*), only a few MCR types' three-dimensional structures have been reported in the PDB database. The modeled full-length MCRs resulting from RoseTTAfold are likely similar to their homolog EptA full-length crystal structure. Such structural data of full-length MCRs could provide a better understanding of catalytic activity than the existing crystal structures and sequence information. Understanding their molecular structures might aid in designing and discovering the inhibitors. Our findings demonstrate that among MCRs, the conserved residues are likely found in the catalytic domain. These residues may be significant in the action of the MCRs family. Four tunnels leading to MCR's active site were discovered for possible PE substrate entering. The most extensive bottleneck radius was obtained in tunnel 1, where the tunnel 1-lining residues were identified in many studies as crucial for substrate binding. The tunnel 1-lining residues for the ligand-binding route shared many conserved residues in all the MCR types and the EptA as they flowed through the critical active site residues. It was consistent with the docking results of most MCRs that the PE docked structures were likely in the located tunnel 1. Its PEA group was posed in the catalytic domain, while the long-chain fatty acid was situated in the transmembrane region. These findings suggest the pathway for substrate binding on MCRs protein, which could be helpful for future MCR inhibitor research.

Appendix A. Supplementary data

Supplementary data associated with this article can be found at http://dx.doi.org/10.2306/scienceasia1513-1874.2022.152.

Acknowledgements: CH thanks the Science Achievement Scholarship of Thailand for the PhD scholarship and the 90th Anniversary of Chulalongkorn University Fund (Ratchadaphiseksomphot Endowment Fund, *GCUGR1125623025D*). PM and TR would like to thank the Foreign Expert Funding of China (Funding ID G2021013001L) for its partial support.

REFERENCES

1. Ma F, Xu S, Tang Z, Li Z, Zhang L (2021) Use of antimicrobials in food animals and impact of transmission of antimicrobial resistance on humans. *Biosaf Health* **3**, 32–38.
2. Hutchings MI, Truman AW, Wilkinson B (2019) Antibiotics: past, present and future. *Curr Opin Microbiol* **51**, 72–80.
3. Nation RL, Li J (2009) Colistin in the 21st century. *Curr Opin Infect Dis* **22**, 535–543
4. Andrade BGN, Goris T, Afli H, Coutinho FH, Dávila AMR, Cuadrat RRC (2021) Putative mobilized colistin resistance genes in the human gut microbiome. *BMC Microbiol* **21**, 220.
5. El-Sayed Ahmed MAE-G, Zhong L-L, Shen C, Yang Y, Doi Y, Tian G-B (2020) Colistin and its role in the Era of antibiotic resistance: an extended review (2000–2019). *Emerg Microbes Infect* **9**, 868–885.
6. Gharaibeh MH, Shatnawi SQ (2019) An overview of colistin resistance, mobilized colistin resistance genes dissemination, global responses, and the alternatives to colistin: A review. *Vet World* **12**, 1735–1746.
7. Li H, Wang Y, Chen Q, Xia X, Shen J, Wang Y, Shao B (2021) Identification of functional interactome of colistin resistance protein MCR-1 in *Escherichia coli*. *Front Microbiol* **11**, 583185.
8. Yang Q, Li M, Spiller O, Andrey D, Hinchliffe P, Li H, Maclean C, Niumsup P, et al (2017) Balancing *mcr-1* expression and bacterial survival is a delicate equilibrium between essential cellular defence mechanisms. *Nat Commun* **8**, 2054.
9. Janssen AB, van Schaik W (2021) Harder, better, faster, stronger: Colistin resistance mechanisms in *Escherichia coli*. *PLoS Genet* **17**, e1009262.
10. Hussein NH, Al-Kadmy IMS, Taha BM, Hussein JD (2021) Mobilized colistin resistance (*mcr*) genes from 1 to 10: a comprehensive review. *Mol Biol Rep* **48**, 2897–2907.
11. Bertelloni F, Cagnoli G, Turchi B, Ebani VV (2022) Low level of colistin resistance and *mcr* genes presence in *Salmonella* spp.: evaluation of isolates collected between 2000 and 2020 from animals and environment. *Antibiotics* **11**, 272.
12. Anandan A, Evans GL, Condic-Jurkic K, O'Mara ML, John CM, Phillips NJ, Jarvis GA, Wills SS, et al (2017) Structure of a lipid A phosphoethanolamine transferase suggests how conformational changes govern substrate binding. *Proc Natl Acad Sci USA* **114**, 2218–2223.

13. Baek M, DiMaio F, Anishchenko I, Dauparas J, Ovchinnikov S, Lee GR, Wang J, Cong Q, et al (2021) Accurate prediction of protein structures and interactions using a three-track neural network. *Science* **373**, 871–876.
14. Altschul SF, Gish W, Miller W, Myers EW, Lipman DJ (1990) Basic local alignment search tool. *J Mol Biol* **215**, 403–410.
15. Robert X, Gouet P (2014) Deciphering key features in protein structures with the new ENDscript server. *Nucleic Acids Res* **42**, W320–W324.
16. Pettersen EF, Goddard TD, Huang CC, Meng EC, Couch GS, Croll TI, Morris JH, Ferrin TE (2021) UCSF ChimeraX: Structure visualization for researchers, educators, and developers. *Protein Sci* **30**, 70–82.
17. Lin Y-F, Cheng C-W, Shih C-S, Hwang J-K, Yu C-S, Lu C-H (2016) MIB: Metal ion-binding site prediction and docking server. *J Chem Inf Model* **56**, 2287–2291.
18. Hinchliffe P, Yang QE, Portal E, Young T, Li H, Tooke CL, Carvalho MJ, Paterson NG, et al (2017) Insights into the mechanistic basis of plasmid-mediated colistin resistance from crystal structures of the catalytic domain of MCR-1. *Sci Rep* **7**, 39392.
19. Chovancova E, Pavelka A, Benes P, Strnad O, Brezovsky J, Kozlikova B, Gora A, Sustr V, et al (2012) CAVER 3.0: A tool for the analysis of transport pathways in dynamic protein structures. *PLoS Comput Biol* **8**, e1002708.
20. Stourac J, Vavra O, Kokkonen P, Filipovic J, Pinto G, Brezovsky J, Damborsky J, Bednar D (2019) Caver Web 1.0: identification of tunnels and channels in proteins and analysis of ligand transport. *Nucleic Acids Res* **47**, W414–W422.
21. Sterling T, Irwin JJ (2015) ZINC 15 – ligand discovery for everyone. *J Chem Inf Model* **55**, 2324–2337.
22. Uddin MB, Alam MN, Hasan M, Hossain SMB, Debnath M, Begum R, Samad MA, Hoque SF, et al (2022) Molecular detection of colistin resistance *mcr-1* gene in multidrug-resistant *Escherichia coli* isolated from chicken. *Antibiotics* **11**, 97.
23. Grosdidier A, Zoete V, Michielin O (2011) SwissDock, a protein-small molecule docking web service based on EADock DSS. *Nucleic Acids Res* **39**, W270–W277.
24. Pettersen EF, Goddard TD, Huang CC, Couch GS, Greenblatt DM, Meng EC, Ferrin TE (2004) UCSF Chimera: a visualization system for exploratory research and analysis. *J Comput Chem* **25**, 1605–1612.
25. Laskowski RA, Swindells MB (2011) LigPlot+: multiple ligand-protein interaction diagrams for drug discovery. *J Chem Inf Model* **51**, 2778–2786.
26. Liu YY, Wang Y, Walsh TR, Yi LX, Zhang R, Spencer J, Doi Y, Tian G, et al (2016) Emergence of plasmid-mediated colistin resistance mechanism MCR-1 in animals and human beings in China: a microbiological and molecular biological study. *Lancet Infect Dis* **16**, 161–168.
27. Wang C, Feng Y, Liu L, Wei L, Kang M, Zong Z (2020) Identification of novel mobile colistin resistance gene *mcr-10*. *Emerg Microbes Infect* **9**, 508–516.
28. Coates K, Walsh TR, Spencer J, Hinchliffe P (2017) 1.12 Å resolution crystal structure of the catalytic domain of the plasmid-mediated colistin resistance determinant MCR-2. *Acta Crystallogr F Struct Biol Commun* **73**, 443–449.
29. Sun J, Xu Y, Gao R, Lin J, Wei W, Srinivas S, Li D, Yang R-S, et al (2017) Deciphering MCR-2 colistin resistance. *mBio* **8**, e00625-17.
30. Hu M, Guo J, Cheng Q, Yang Z, Chan E, Chen S, Hao Q (2016) Crystal structure of *Escherichia coli* originated MCR-1, a phosphoethanolamine transferase for colistin resistance. *Sci Rep* **6**, 38793.
31. Gao R, Hu Y, Li Z, Sun J, Wang Q, Lin J, Ye H, Liu F, et al (2016) Dissemination and mechanism for the MCR-1 colistin resistance. *PLoS Pathog* **12**, e1005957.
32. Hinchliffe P, Yang QE, Portal E, Young T, Li H, Tooke CL, Carvalho MJ, Paterson NG, et al (2017) Insights into the mechanistic basis of plasmid-mediated colistin resistance from crystal structures of the catalytic domain of MCR-1. *Sci Rep* **7**, 9392.
33. Ma G, Zhu Y, Yu Z, Ahmad A, Zhang H (2016) High resolution crystal structure of the catalytic domain of MCR-1. *Sci Rep* **6**, 39540.
34. Stojanoski V, Sankaran B, Prasad BV, Poirel L, Nordmann P, Palzkill T (2016) Structure of the catalytic domain of the colistin resistance enzyme MCR-1. *BMC Biol* **14**, 81.
35. Wei P, Song G, Shi M, Zhou Y, Liu Y, Lei J, Chen P, Yin L (2018) Substrate analog interaction with MCR-1 offers insight into the rising threat of the plasmid-mediated transferable colistin resistance. *FASEB J* **32**, 1085–1098.
36. Sun H, Zhang Q, Wang R, Wang H, Wong YT, Wang M, Hao Q, Yan A, et al (2020) Resensitizing carbapenem- and colistin-resistant bacteria to antibiotics using auranofin. *Nat Commun* **11**, 5263.
37. Wang X, Lu Q, Qi J, Chai Y, Wang Y, Gao GF (2018) Structural and functional insights into MCR-2 mediated colistin resistance. *Sci China Life Sci* **61**, 1432–1436.
38. Lythell E, Suardíaz R, Hinchliffe P, Hanpaibool C, Visitsatthawong S, Oliveira ASF, Lang EJM, Surawatanawong P, et al (2020) Resistance to the "last resort" antibiotic colistin: a single-zinc mechanism for phosphointermediate formation in MCR enzymes. *Chem Commun (Camb)* **56**, 6874–6877.
39. Liu Z-X, Han Z, Yu X-L, Wen G, Zeng C (2018) Crystal structure of the catalytic domain of MCR-1 (cMCR-1) in complex with d-xylose. *Crystals* **8**, 172.
40. Xu Y, Lin J, Cui T, Srinivas S, Feng Y (2018) Mechanistic insights into transferable polymyxin resistance among gut bacteria. *J Biol Chem* **293**, 4350–4365.
41. Son SJ, Huang R, Squire CJ, Leung IKH (2019) MCR-1: a promising target for structure-based design of inhibitors to tackle polymyxin resistance. *Drug Discov Today* **24**, 206–216.
42. Colthart AM, Tietz DR, Ni Y, Friedman JL, Dang M, Pochapsky TC (2016) Detection of substrate-dependent conformational changes in the P450 fold by nuclear magnetic resonance. *Sci Rep* **6**, 22035.
43. Jain S, Sekhar A (2022) Elucidating the mechanisms underlying protein conformational switching using NMR spectroscopy. *J Magn Reson Open* **10–11**, 100034.
44. Nicolaï A, Delarue P, Senet P (2013) Decipher the mechanisms of protein conformational changes induced by nucleotide binding through free-energy landscape analysis: ATP binding to Hsp70. *PLoS Comput Biol* **9**, e1003379.

Appendix A. Supplementary data

	MCR-1	MCR-2	MCR-3	MCR-4	MCR-5	MCR-6	MCR-7	MCR-8	MCR-9	MCR-10
MCR-1										
MCR-2	81.3									
MCR-3	35.3	35.1								
MCR-4	33.9	34.8	48.7							
MCR-5	39.7	37.7	35.1	34.8						
MCR-6	82.8	87.9	34.5	33.0	38.7					
MCR-7	36.1	34.5	71.6	45.0	38.7	33.9				
MCR-8	33.7	32.8	43.8	40.0	37.0	33.8	42.2			
MCR-9	36.3	33.9	64.7	43.2	33.4	33.5	62.5	44.8		
MCR-10	36.3	34.6	62.1	44.7	36.6	34.2	59.9	43.4	82.9	

Fig. S1 Percentage identity matrix for protein sequence alignments for all the ten MCR proteins.

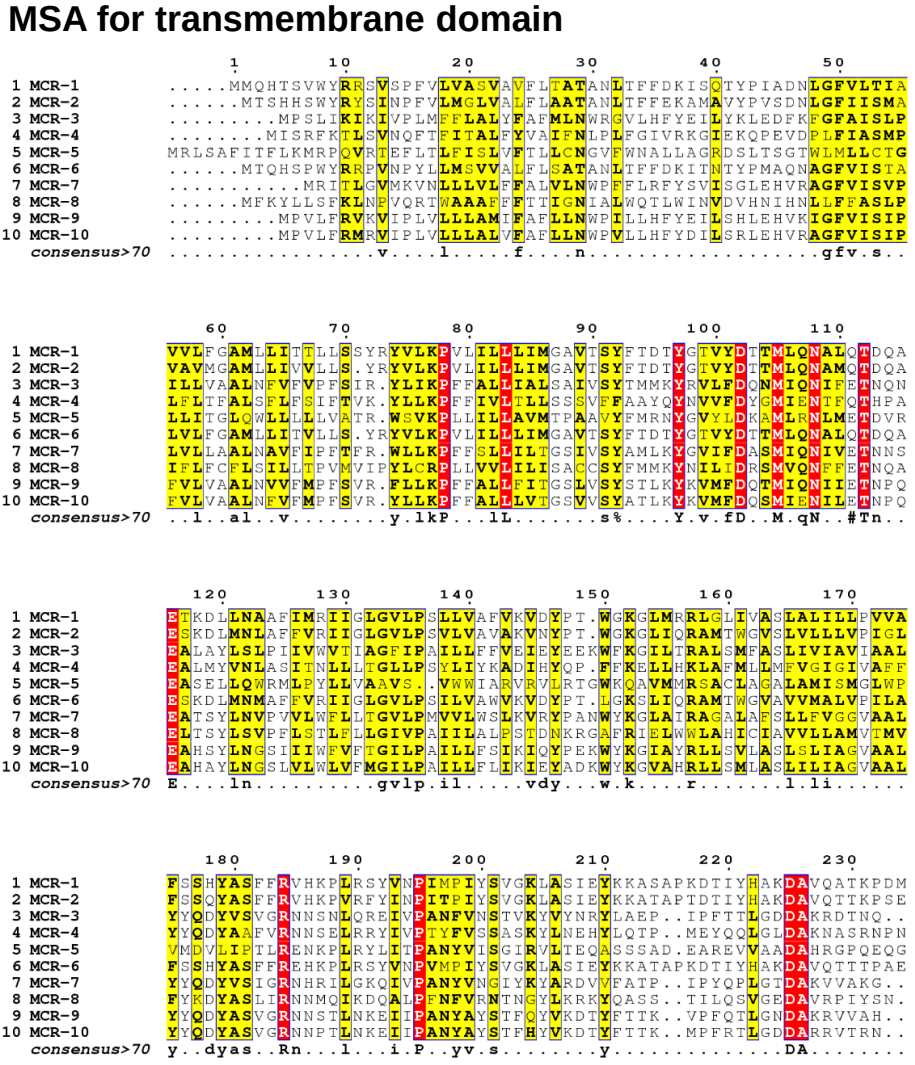

Fig. S2 Multiple sequence alignment (MSA) of MCR-1 to 10 proteins on the transmembrane domain with the highlight consensus residues.

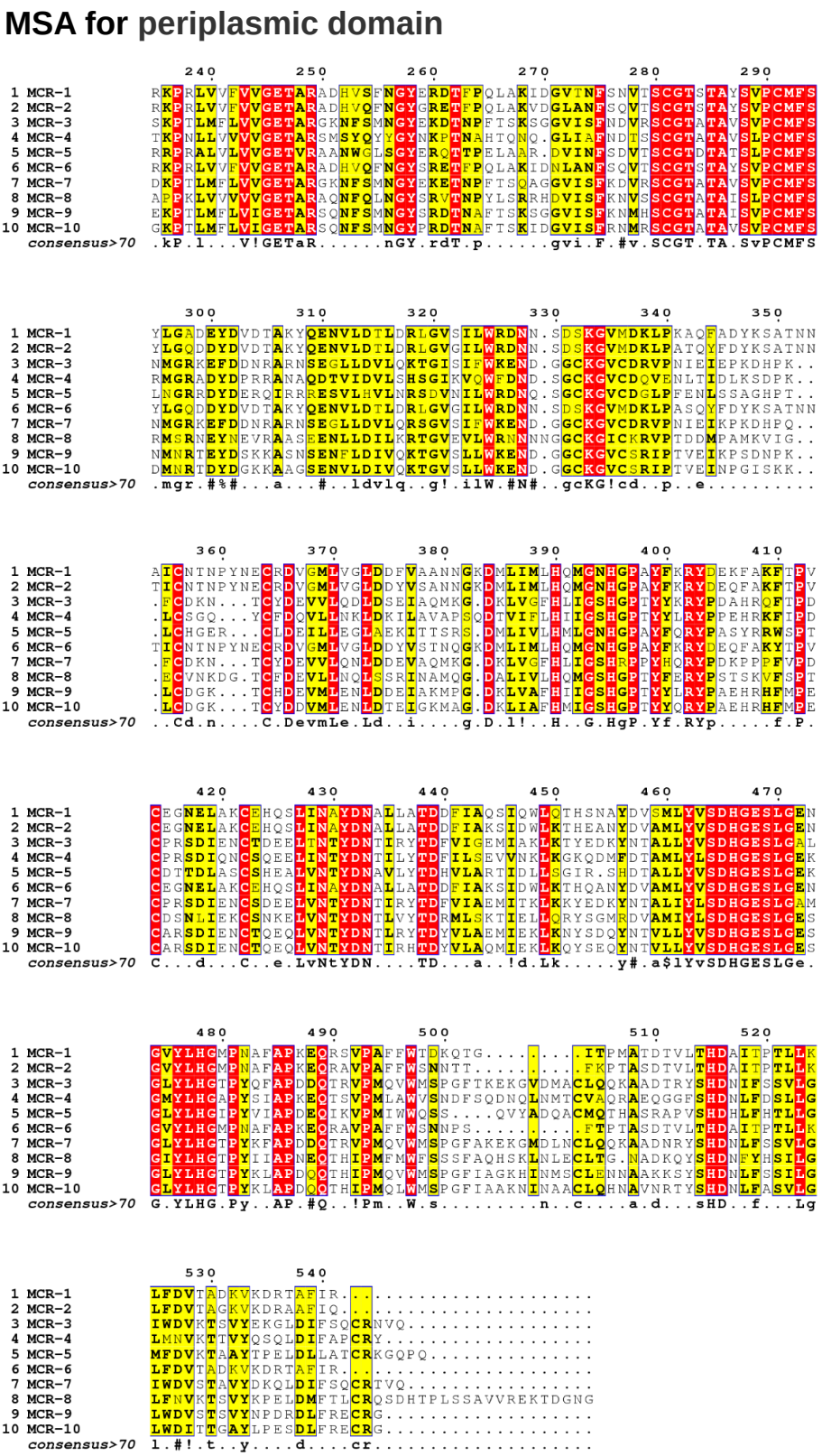

Fig. S3 Multiple sequence alignment (MSA) of MCR-1 to 10 proteins on the periplasmic domain with the highlight consensus residues.

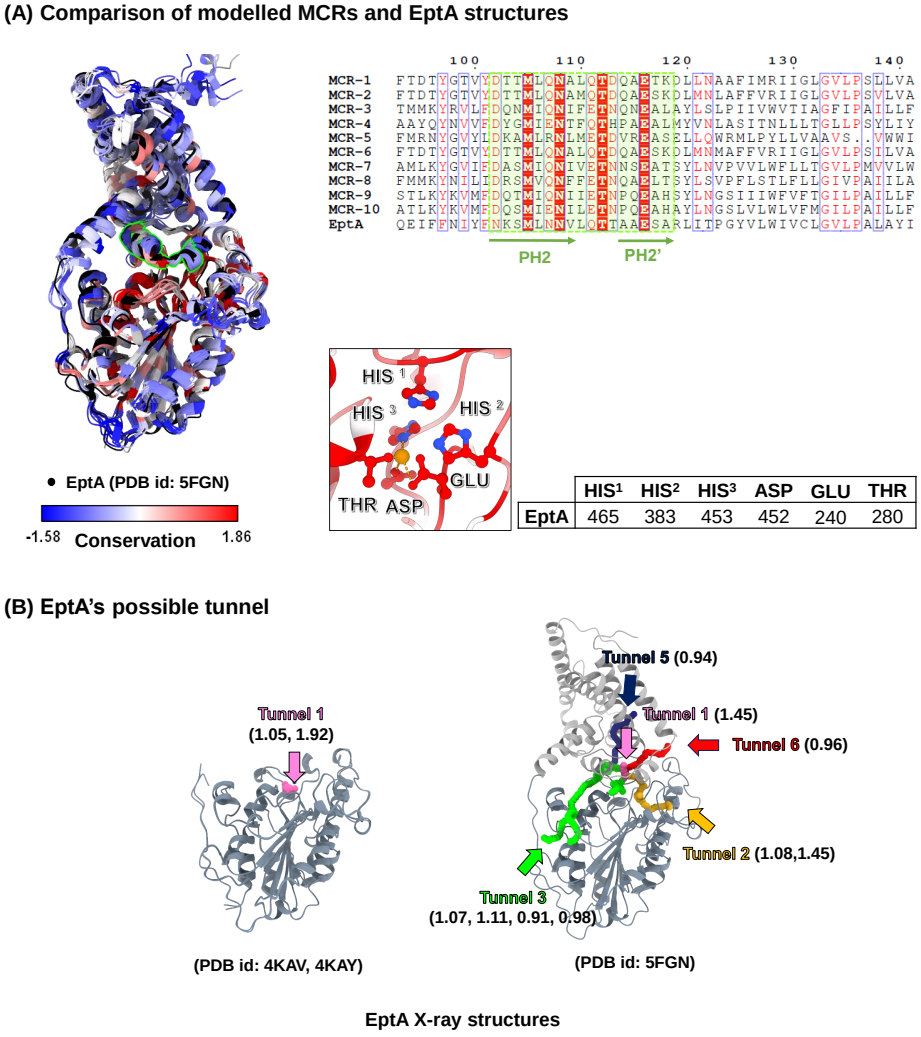

Fig. S4 (A) Superimposed structures of modeled MCRs (MCR-1 to 10) and EptA's X-ray structure where the comparison of PH2/PH2' sequences in right side were outlined in green on superimposed structures. (B) Possible tunnels of EptA X-ray structure where their bottleneck radii are given in the bracket.

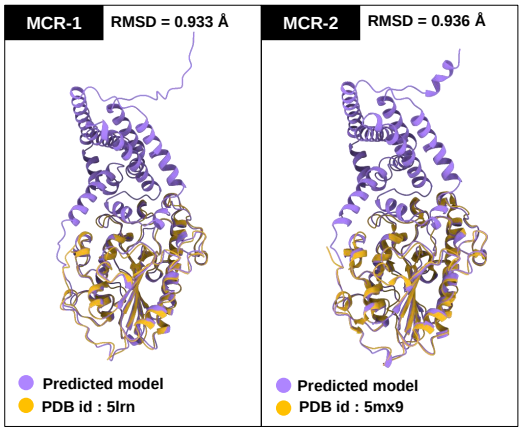

Fig. S5 Superimposed structures of the periplasmic domain between the predicted models by RoseTTAfold and the crystal structures of MCR-1 and MCR-2.

Amino acid	MCR-1	Amino acid	MCR-2	Amino acid	MCR-3	Amino acid	MCR-4	Amino acid	MCR-5	Amino acid	MCR-6	Amino acid	MCR-7	Amino acid	MCR-8	Amino acid	MCR-9	Amino acid	MCR-10
L	69							V	74										
						I	77	I	85										
L	82							L	86	L	80	L	75	V	81	L	77	L	77
																L	78		
I	85	I	83			L	81			I	83			L	84	I	80		
M	86	M	84	L	81	L	82	M	90	M	84			I	85	T	81		
V	89	V	87	I	84	S	85	A	93	V	87	I	82	C	88	L	84		
		T												C	89				
F	93	F	91	T	88			F	97	F	91								
Y	101	Y	99	F	96	F	97			Y	99					F	96		
M	105	M	103			M	101									M	100		
										L	104								
N	108	N	106			N	104									N	103		
A	109	A	107	I	104	T	105	L	113	A	107	I	102	F	108	I	104	I	104
										L	108	V	103	F	109				
T	112	T	110			T	108	T	116	T	110	T	105			T	107		
												N	107					P	109
T	117			A	112	A	113	A	121	S	115	A	110	L	116			A	112
				L	113													H	113
L	120	L	118	Y	115	Y	116					Y	113	Y	119	Y	115	Y	115
				L	116	V	117	L	125	M	119	L	114	L	120	L	116	L	116
						S	121	M	129	F	123	V	118						
				V	124							F	122			F	124	L	124
				T	125														
		V	132	F	129					V	132					I	129	I	129
										S	135								
L	138			I	133					I	136								
																		F	136
				F	194			Y	201					F	198	Y	194		
I	199	I	197					V	202					V	199				
H	395	H	393																
		L	475													L	462		
		H	476													H	463		

Fig. S6 List of interacting MCR residues with the PE substrate extracted from Fig. 5.

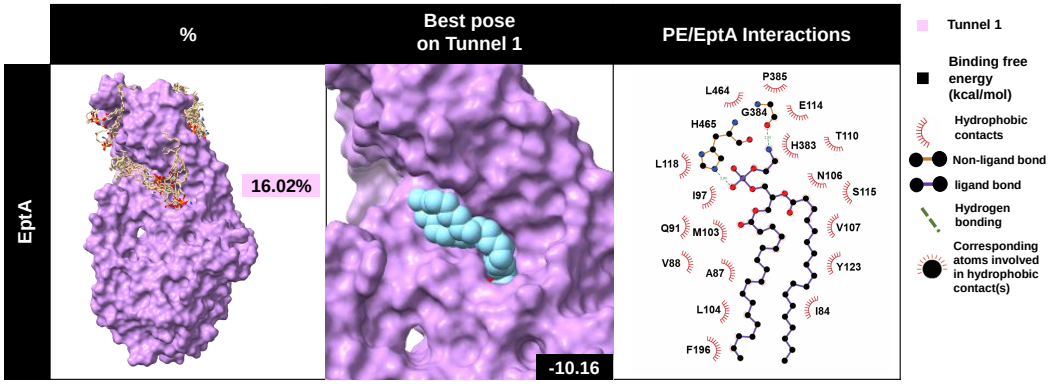

Fig. S7 The percentage of PE substrate binding to the tunnels 1 with the best docked pose on the tunnel 1 retrieved by blind docking simulation on the EptA (PDB id: 5FGN) using the SwissDock server [23] where the substrate-protein interactions are depicted on right site.